Article ID: 1000-324X(2021)12-1323-07 **DOI:** 10.15541/jim20210206

Symmetrical La^{3+}-doped $Sr_2Fe_{1.5}Ni_{0.1}Mo_{0.4}O_{6-\delta}$ Electrode Solid Oxide Fuel Cells for Pure CO_2 Electrolysis

WANG Yue[1,2], CUI Changsong[1,2], WANG Shiwei[1,2], ZHAN Zhongliang[1,2,3]

(1. Shanghai Institute of Ceramics, Chinese Academy of Sciences, Shanghai 200050, China; 2. University of Chinese Academy of Sciences, Beijing 100049, China; 3. School of Chemistry and Materials Science, University of Science & Technology of China, Hefei 230026, China)

Abstract: Electrochemical reduction of the greenhouse gas CO_2 in solid oxide electrolysis cells (SOECs) has attracted much attention due to their high energy conversion efficiency and great potential for carbon cycling. Compared with the asymmetrical configuration, symmetrical SOECs with the same material as anode and cathode, can greatly simplify the fabrication process and reduce the complication associated with varied interfaces. Perovskite oxides $La_xSr_{2-x}Fe_{1.5}Ni_{0.1}Mo_{0.4}O_{6-\delta}$ (L_xSFNM, x=0.1, 0.2, 0.3 and 0.4) are prepared and evaluated as symmetrical electrodes in solid oxide electrolysis cells for electrochemical reduction of pure CO_2. The polarization resistances are 0.07 $\Omega\cdot cm^2$ in air and 0.62 $\Omega\cdot cm^2$ in 50% CO-50% CO_2 for $L_{0.3}$SFNM electrode at 800 ℃. An electrolysis current density of 1.17 $A\cdot cm^{-2}$ under 800 ℃ at 1.5 V is achieved for the symmetrical SOECs in pure CO_2. Furthermore, the symmetrical cell demonstrates excellent stability during the preliminary 50 h CO_2 electrolysis measurements.

Key words: symmetrical solid oxide electrolysis cells; perovskite; electrode materials

In the past seventy years, the concentration of CO_2 in atmosphere has increased by about 0.012%, which is the main reason of greenhouse effect inducing a series of problems like global warming and climate change[1]. Capture and utilization of CO_2 is of great significance to sustainable development of human society. Nevertheless, high thermodynamic stability and kinetic inertness of CO_2 limit its conversion and applications[2]. Solid oxide electrolysis cells (SOECs) are one of the most promising technologies to convert CO_2 into high energy density fuels and value-added chemicals using the surplus renewable electricity, promoting CO_2 utilization and penetration of renewable electricity in the current energy regime as well[3-4].

Ni-based cermets are the commonly used cathodes in SOECs, but suffer from some limitations such as nickel oxidation in CO_2-rich atmospheres and carbon deposition in CO-rich atmosphere at high CO_2 conversions, which may prevent their practical applications[5-6]. Due to their distinctive features such as brilliant redox stability and excellent resistance against coking formation and sulfur poisoning, mixed ionic-electronic conducting oxides have been widely investigated as alternative cathodes for CO_2 electrolysis. Furthermore, some mixed conducting oxides can be simultaneously used as both anodes and cathodes to obtain symmetrical SOECs, which greatly simplifies the fabrication process and reduces complications associated with the different electrode|electrolyte interfaces. Extensive efforts have been made to explore perovskite and double-perovskite electrodes in symmetrical SOECs, such as $Sr_2Fe_{1.5}Mo_{0.5}O_{6-\delta}$[7-8], $La_{0.75}Sr_{0.25}Cr_{0.5}Mn_{0.5}O_{3-\delta}$[9], $La_xSr_{1-x}TiO_{3-\delta}$[10-11] and $La_{0.6}Sr_{0.4}Fe_{0.8}Ni_{0.2}O_{3-\delta}$[12]. The symmetrical electrodes should be stable with sufficient electrical conductivities (*e.g.*, >1 $S\cdot cm^{-1}$) in both air and fuel environments, and have good chemical compatibility with the other cell components. $La_{0.6}Ca_{0.4}Fe_{0.8}Ni_{0.2}O_{3-\delta}$ (LCaFN) was employed as the electrodes for symmetrical SOECs, showing a self-recovery from the performance degradation due to formation of carbonates by air treatment[13]. $Sr_2Fe_{1.5}Mo_{0.5}O_{6-\delta}$ (SFM), the symmetrical SOFC electrodes developed by Liu, *et al*. exhibited high electrocatalytic activities for both CO_2 reduction and oxygen evolution reactions in symmetrical SOECs[14]. Partial substitution in the A or B site is an effective strategy to optimize the catalytic activity of perovskite oxides. Ce^{4+} was in-

Received date: 2021-03-26; **Revised date:** 2021-04-27; **Published online:** 2021-05-25
Foundation item: National Natural Science Foundation of China (51672298); State Grid Corporation of China (521205200011)
Biography: WANG Yue (1994–), female, PhD candidate. E-mail: wangyue@mail.sic.ac.cn
王 玥(1994–), 女, 博士研究生. E-mail: wangyue@mail.sic.ac.cn
Corresponding author: ZHAN Zhongliang, professor. E-mail: zzhan@ustc.edu.cn
占忠亮, 教授. E-mail: zzhan@ustc.edu.cn

troduced into the A site of $La_{0.7}Sr_{0.3}Cr_{0.5}Fe_{0.5}O_{3-\delta}$ (LSCrF) to increase oxygen vacancies in the lattice by *in situ* reduction under the operational conditions and thereby enhance the catalytic activities[15]. In this work, La^{3+} doped $Sr_2Fe_{1.5}Ni_{0.1}Mo_{0.4}O_{6-\delta}$ (L_xSFNM) was investigated as the symmetrical SOEC electrodes for direct CO_2 electrolysis. The influence of the La^{3+} content on the oxygen vacancy concentration, electrical conductivity, and catalytic activity were analyzed. Electrochemical performance was evaluated on symmetrical "L_xSFNM@LSGM|LSGM|L_xSFNM@LSGM" cells for pure CO_2 electrolysis.

1 Experimental

L_xSFNM powders were prepared using the Sol-Gel method. The precursor solution was prepared as follows: stoichiometric amounts of the nitrate salts $La(NO_3)_3{\cdot}6H_2O$, $Sr(NO_3)_2$, $Fe(NO_3)_3{\cdot}9H_2O$, $Ni(NO_3)_3{\cdot}6H_2O$ and $(NH_4)_6Mo_7O_{24}{\cdot}4H_2O$ were firstly dissolved in distilled water, and then citric acid was added with the molar ratio of the citric acid to the total metal ions at 1.2∶1. The precursor solution was subsequently heated at 80 ℃ until a gel was formed, followed by drying at 200 ℃ for 5 h and calcination at 1000 ℃ in air for 5 h to obtain pure L_xSFNM powders.

The tri-layer structure of "porous|dense|porous" LSGM ($La_{0.9}Sr_{0.1}Ga_{0.8}Mg_{0.2}O_{3-\delta}$) was prepared by laminating three tape-cast green tapes at 75 ℃ and 20 MPa, with 40wt% rice starch and graphite used as the pore-forming material in the porous layers. The laminated layers were co-fired at 1380 ℃ to produce the final ceramic structures. L_xSFNM catalysts were added into the porous LSGM scaffolds by impregnating the precursor solution with the total concentration of metal ions at 1 mol·L^{-1}, followed by calcination at 1000 ℃ for 5 h. The impregnation and calcination cycle was repeated for 16 times so as to achieve an L_xSFNM loading of ~25wt% relative to the LSGM scaffolds.

The X-ray diffraction (XRD) pattern of as-synthesized powders was examined at room temperature on an Rigaku D/Max 2100 Powder X-ray Diffractometer with a monochromatic Cu Kα and the diffraction data were recorded in the range 2θ=20°–80° with scan rate of 5 (°)/min. The cell structure was examined using the scanning electron microscope (SEM) in a FEI Magellan 400 microscope. The conductivities of L_xSFNM were tested in air and 50% CO-50% CO_2 using the DC four-probe method. For fuel cell measurements, silver ink (DAD87, Shanghai Institute of Synthetic Resin) and silver wires was applied on the anode and cathode electrode surface as the current collectors. Impedance measurements were performed on the symmetrical fuel cells in a homogeneous environment of air or 50% CO-50% CO_2. The electrolysis performance of the symmetrical fuel cells was evaluated using IM6 Electrochemical Workstation (ZAHNER, Germany), with pure CO_2 fed to the cathodes at 50 sccm and ambient air in the anodes.

2 Results and discussion

The XRD patterns of $La_xSr_{2-x}Fe_{1.5}Ni_{0.1}Mo_{0.4}O_{6-\delta}$ oxides at room temperature are shown in Fig. 1(a). All samples showed a pure cubic perovskite structure without any extra peaks of impurities observed. Fig. 1(b) shows that the (110) peak shifts to a higher scattering angle at x=0.1, which can be explained by smaller ionic radius for La^{3+} than that for Sr^{2+} (0.136 nm *vs.* 0.144 nm). With the La^{3+} content further increasing, the diffraction peak shifted to lower scattering angles. Prior reports showed that the cell expansion was inhibited due to the steric effects associated with anti-site defects[16-17]. This indicates the existence of a disordered crystal structure in L_xSFNM double perovskites.

Fig. 2 compares the thermogravimetric curves of L_xSFNM powders in air, showing a loss of 1%–1.5% in the powder weight due to release of the lattice oxygen with the temperature increasing from 30 to 900 ℃. Note that the largest weight loss was observed for $L_{0.3}$SFNM, indicating the most abundant presence of oxygen vacancies at high temperatures. Fig. 3(a, b) show the conductivities of L_xSFNM measured in air or 50% CO-50% CO_2 at 650–800 ℃. Due to their p-type conducting nature, the conductivities were much higher in air than those in 50% CO-50% CO_2 (17.3–38.1 *vs.* 2.7–5.5 S·cm^{-1}). Fig. 3 also shows that $L_{0.3}$SFNM had the highest conductivities among four samples at all temperatures. For $x \leqslant 0.3$, partial substitution of La^{3+} for Sr^{2+} increased the concentration of anti-site defects and the electron density of Fermi level. It has been reported that the half metallic properties of SFM was quite sensitive to the anti-site defect concentration as it altered the Fe–O–Mo bonding network

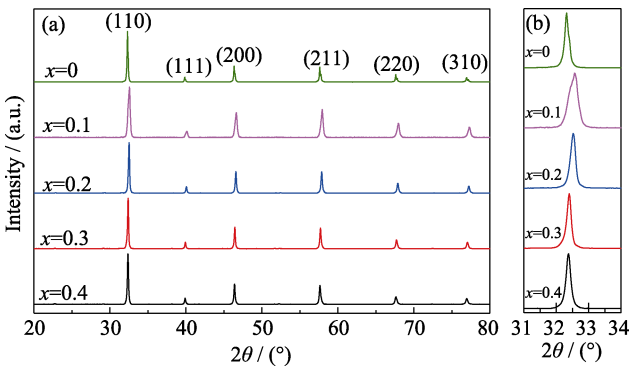

Fig. 1 (a) XRD patterns of L_xSFNM (x=0–0.4) powder calcined at 1000 ℃ in air for 5 h and (b) corresponding magnified patterns within 2θ=31°–35°

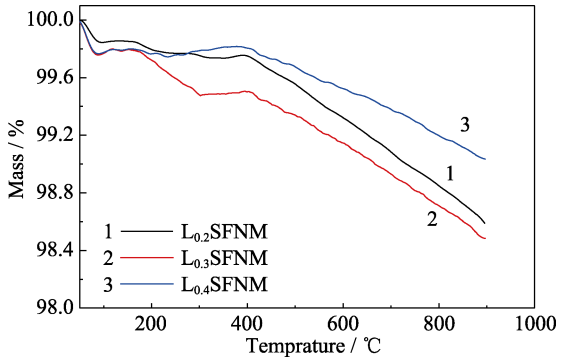

Fig. 2　TGA analysis of L_xSFNM in air

and the electronic hopping pathway[18]. Due to a decrease in the crystal symmetry and the cation order, the double exchange interaction between Fe–O–Mo may be inhibited at $x \geqslant 0.4$, leading to decreased conductivities[19-21].

In order to study the effect of different La^{3+} contents on the activities of L_xSFNM oxides toward oxygen evolution and CO_2 reduction reactions, electrochemical impedance measurements were performed on electrolyte-supported symmetrical cells with impregnated L_xSFNM electrodes, *i.e.*, L_xSFNM@LSGM|LSGM|L_xSFNM@LSGM (Fig. 4(a)). The dense LSGM electrolytes were 210 μm in thickness, whereas the porous electrodes were around 20 μm in thickness. Fig. 4(b) shows excellent interfacial bonding between dense electrolytes and the porous scaffolds that is conducive to minimizing the contact resistance. As shown in Fig. 4(c), nano-scale L_xSFNM catalysts were deposited onto the internal surfaces of porous LSGM scaffolds to form a well-interconnected network to facilitate electronic conduction and thus enhance their catalytic activities.

Electrochemical impedance measurements were performed for symmetrical cells in the homogeneous environment of dry air or 50% CO-50% CO_2, with the typical Nyquist plots of impedance data as compared in Fig. 5. Note that the electrolyte resistances were subtracted from the cell impedance, and the polarization resistances were divided by two due to the symmetrical configurations. Fig. 5(a) shows that the anode polarization resistances ($R_{P,A}$) at 800 ℃ are 0.12, 0.09, 0.07 and 0.10 Ω·cm^2 for $L_{0.1}$SFNM, $L_{0.2}$SFNM, $L_{0.3}$SFNM and $L_{0.4}$SFNM in dry air, respectively. $L_{0.3}$SFNM exhibited much smaller $R_{P,A}$ compared with some previously reported air electrodes, such as Sr_2FeMoO_6 (0.1 Ω·cm^2 at 850 ℃)[22], $Sr_2Fe_{1.4}Ni_{0.1}Mo_{0.5}O_{6-\delta}$ (0.22 Ω·cm^2 at 750 ℃)[23], $Pr_{0.6}Sr_{0.4}Fe_{0.7}Ni_{0.1}Mo_{0.1}O_{3-\delta}$ (0.4 Ω·cm^2 at 800 ℃)[24] and $La_{0.6}Sr_{0.4}Fe_{0.9}Mn_{0.1}O_{3-\delta}$-GDC (0.24 Ω·cm^2 at 800 ℃)[25]. Distribution of relaxation time (DRT) analyses were conducted on impedance data so as to identify the number of polarization processes involved in the oxygen evolution reaction. With spectra transferred from the frequency into time domain, the overlapped polarization processes can be clearly distinguished. Fig. 5(b) shows that all DRT curves have three distinctive peaks, corresponding to three elementary reaction processes in the oxygen evolution

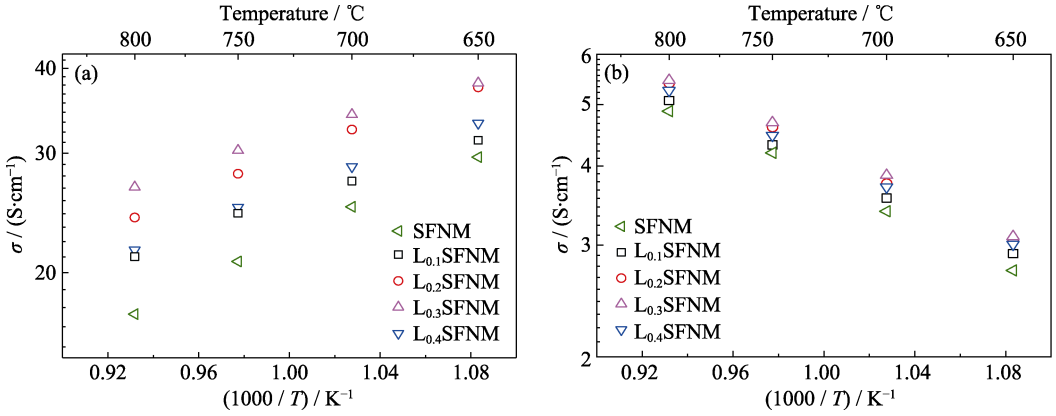

Fig. 3　Electricity conductivities of L_xSFNM at 650-800 ℃ in (a) air and (b) 50% CO-50% CO_2

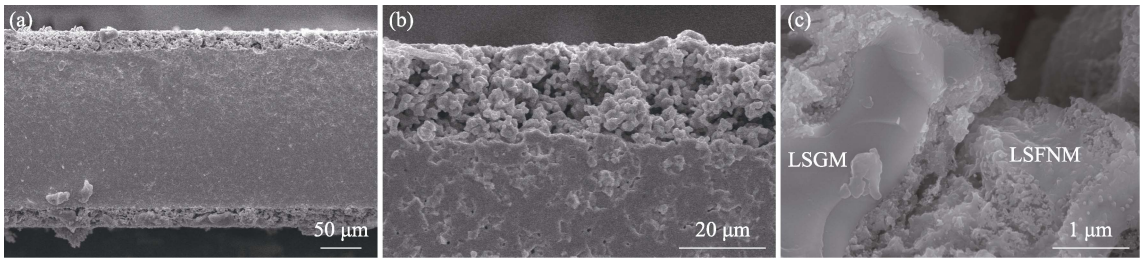

Fig. 4　(a) Cross-sectional SEM image of the tri-layer symmetrical structure of "porous|dense|porous" LSGM and (b) high magnification view of symmetrical cell, and (c) high-magnification view of impregnated $L_{0.3}$SFNM catalyst

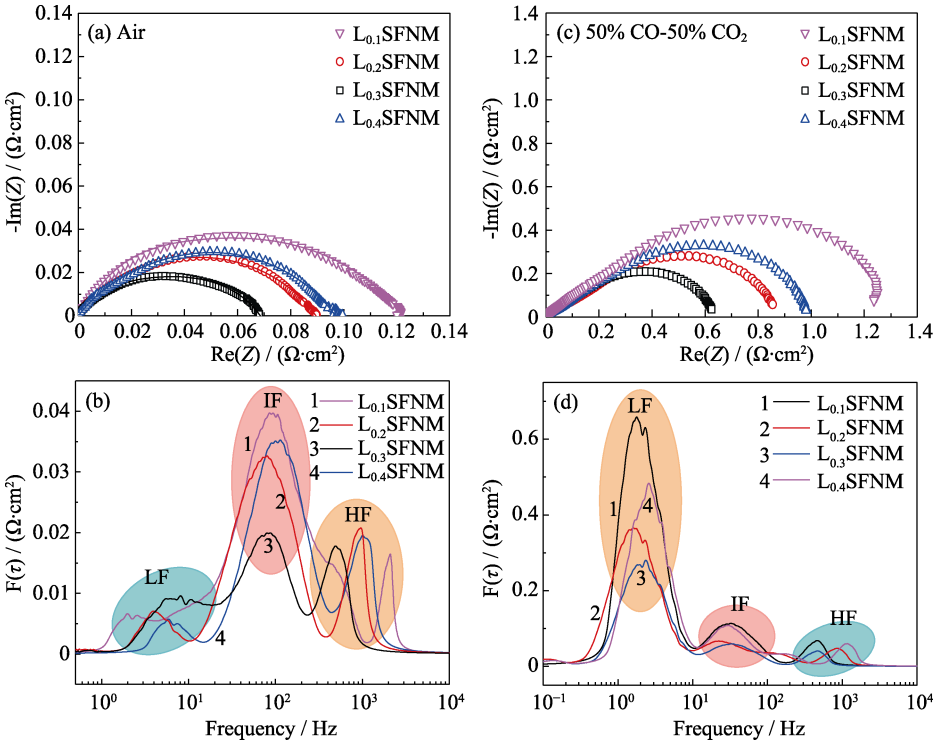

Fig. 5 Nyquist plots of impedance data measured with L_xSFNM at 800 ℃ in (a) air and (c) 50% CO-50% CO_2; (b, d) DRT curves of impedance data shown in (a, c)

reaction. The low-frequency peaks (1–10 Hz) were usually assigned to gas diffusion in the porous electrodes, while the high frequency peaks (300–2000 Hz) were related to the charge transfer process across the electrode-electrolyte interfaces. R_{LF} and R_{HF} were almost independent of the La^{3+} content. Note that the intermediate frequency peaks (50–200 Hz) dropped pronouncedly in the order of $L_{0.1}SFNM > L_{0.4}SFNM > L_{0.2}SFNM > L_{0.3}SFNM$. Given that the intermediate frequency peaks were usually associated with the bulk transport of oxygen surface exchange and O^{2-} bulk diffusion[26], it can be concluded that $L_{0.3}SFNM$ had the highest surface oxygen exchange rate. The highest activity of $L_{0.3}SFNM$ toward oxygen evolution was also consistent with the smallest activation energy of $R_{P,A}$ among the investigated L_xSFNM (Fig. 6(a)). It should also be pointed out that the intermediate frequency peaks were much larger than the low- or high-frequency peaks for all L_xSFNM samples, indicating that surface oxygen exchange is the rate-limiting step in oxygen evolution reaction.

Fig. 5(c) shows an order of the cathode polarization resistances ($R_{P,C}$) - $L_{0.3}SFNM$ (0.62 Ω·cm^2)<$L_{0.2}SFNM$ (0.86 Ω·cm^2) < $L_{0.4}SFNM$ (0.98 Ω·cm^2) < $L_{0.1}SFNM$ (1.24 Ω·cm^2) measured in 50% CO-50% CO_2, demonstrating that $L_{0.3}SFNM$ had the highest activities toward CO_2 reduction reactions. Fig. 5(d) shows the DRT analysis results of impedance data in Fig. 5(c), also showing three well distinguished peaks. The low-, intermediate- and high-frequency peaks were associated with dissociative adsorption of CO_2 molecules on the surface, surface

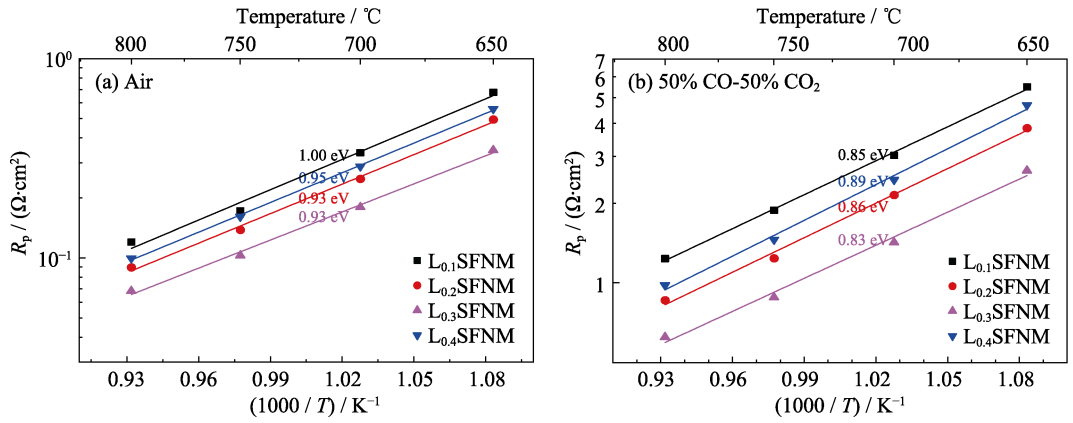

Fig. 6 Measured polarization resistances *versus* the temperature reciprocal in (a) air and (b) 50% CO-50% CO_2

diffusion and the charge transfer process, respectively. R_{HF} and R_{IF} remained independent of the La^{3+} content, while R_{LF} showed the lowest at x=0.3. Much higher R_{LF} than R_{HF} and R_{IF} indicated that the overall CO_2 electroreduction was limited by dissociative adsorption of CO_2 on the surface of LSFNM. Moreover, the cathode polarization resistances ($R_{P,C}$) was much larger than $R_{P,A}$, demonstrating that the electrochemical performance of the CO_2 electrolysis cells mainly depended on the catalytic activities of cathodes toward CO_2 reduction reactions. Fig. 6(b) shows that the activation energies of $R_{P,C}$ are 0.83–0.89 eV.

The electrochemical performance of $L_{0.3}$SFNM electrode for pure CO_2 electrolysis was further evaluated using the LSGM-electrolyte supported SOECs at 650–800 ℃, with pure CO_2 in the cathodes at 50 sccm and ambient air in the anodes. Fig. 7(a) shows the curves of measured voltages as a function of current densities. At the applied voltage of 1.5 V, the electrolysis current densities increased from 0.4 A·cm^{-2} at 650 ℃ to 1.17 A·cm^{-2} at 800 ℃. These values were competitive when compared with previously reported results listed in Table 1. Fig. 7(b) compares the corresponding EIS spectra measured at 1.5 V. The Ohmic resistance and polarization resistance both

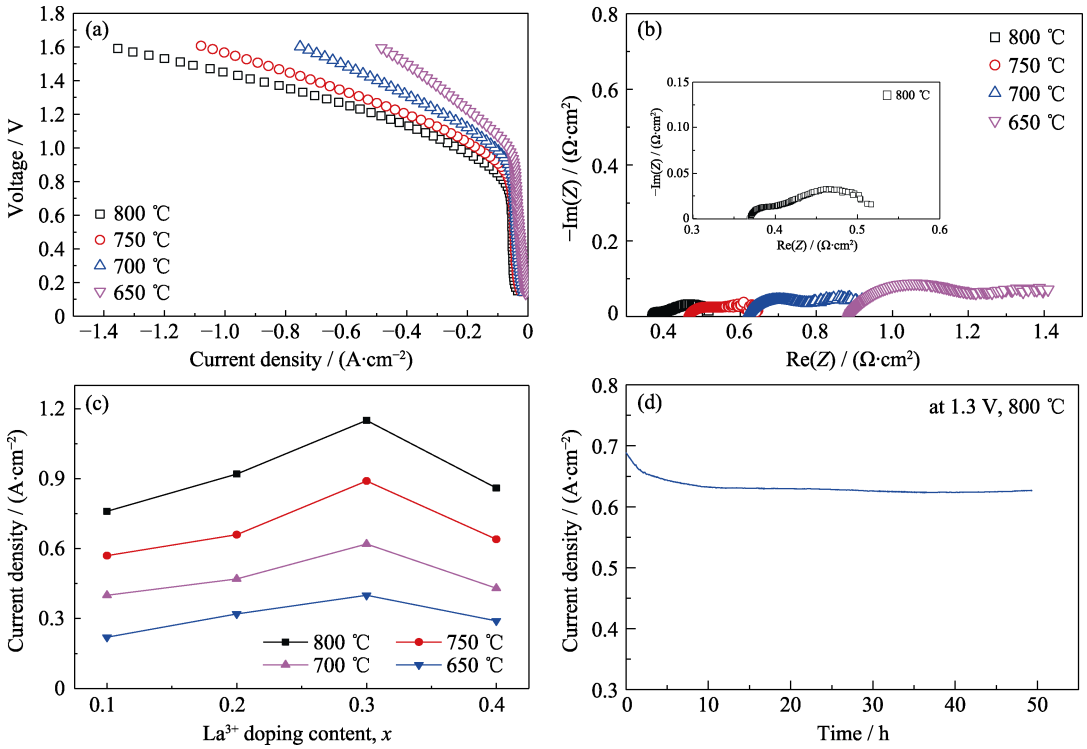

Fig. 7　(a) *I-V* curves and (b) impedance spectra measured at the 1.5 V of a single electrolyte-supported electrolysis cell with $L_{0.3}$SFNM at different temperatures with inset in (b) showing corresponding enlarged spectrum of the cell with $L_{0.3}$SFNM at 800 ℃, (c) current densities with varied La_xSFNM anodes at 1.5 V under different temperatures, and (d) short-term stability test of the symmetrical SOECs with $L_{0.3}$SFNM electrode, operating under 800 ℃ at an applied voltage of 1.3 V

Table 1　Comparison of literature values of current densities achieved for pure CO_2 electrolysis in electrolyte-supported cells at 1.5 V under 800 ℃

Electrode	Electrolyte	Performance/(A·cm^{-2})	Ref.
$La_{0.3}Sr_{0.7}Fe_{0.7}Ti_{0.3}O_3$	YSZ	0.52 (2V)	[27]
$La_{0.6}Sr_{0.4}Fe_{0.9}Mn_{0.1}O_{3-\delta}$-GDC	YSZ	1.107 (2V)	[25]
$La_{0.6}Sr_{0.4}Fe_{0.8}Ni_{0.2}O_{3-\delta}$-GDC	YSZ	1.03	[28]
$La_{0.4}Sr_{0.6}Co_{0.2}Fe_{0.7}Nb_{0.1}O_{3-\delta}$	YSZ	0.442	[29]
$La_{0.6}Ca_{0.4}Fe_{0.8}Ni_{0.2}O_{3-\delta}$-GDC	YSZ	0.78	[13]
$La_{0.75}Sr_{0.25}Cr_{0.5}Mn_{0.5}O_{3-\delta}$	YSZ	0.09	[30]
$La_{0.3}Sr_{0.7}Cr_{0.3}Fe_{0.7}O_{3-\delta}$	YSZ	0.32	[31]
$(PrBa)_{0.95}(Fe_{0.9}Mo_{0.1})_2O_{5+\delta}$	LSGM	0.51 (1.3V)	[32]
$La_{0.3}Sr_{1.7}Fe_{1.5}Ni_{0.1}Mo_{0.4}O_{6-\delta}$	LSGM	1.17	This work

YSZ=$Zr_{0.84}Y_{0.16}O_{1.92}$; GDC=$Gd_{0.9}Ce_{0.1}O_{2-\delta}$; LSGM=$La_{0.9}Sr_{0.1}Ga_{0.8}Mg_{0.2}O_{3-\delta}$

increased obviously with reduced cell operating temperature. The interfacial polarization resistances were 0.13 Ω·cm^2 at 800 ℃ and 0.52 Ω·cm^2 at 650 ℃. Fig. 7(c) summarizes the correlation between the doping amount of La^{3+} ions and the electrolysis current density at 1.5 V, showing that $L_{0.3}$SFNM yielded the highest performance at all measurement temperatures. Fig. 7(d) shows the preliminary short-term stability of symmetrical $L_{0.3}$SFNM electrode cells measured at 800 ℃ and 1.3 V in pure CO_2. The current density slightly dropped from 0.68 to 0.64 A·cm^{-2} during the first 2 h, and then remained stable, indicating good stability of the nano-scale $L_{0.3}$SFNM electrodes.

3 Conclusions

In summary, a series of perovskite oxides $La_xSr_{2-x}Fe_{1.5}Ni_{0.1}Mo_{0.4}O_{6-\delta}$ (L_xSFNM, x=0.1, 0.2, 0.3 and 0.4) have been synthesized and evaluated as symmetrical electrodes for solid oxide electrolysis cells. Impedance measurements show that the electrode performance strongly depended upon the La^{3+} doping content in L_xSFNM. Both of the highest activities for oxygen evolution and CO_2 reduction observed both at x=0.3. LSGM electrolyte-supported SOECs produce an electrolysis current density of 1.17 A·cm^{-2} at 800 ℃ and 1.5 V in pure CO_2, and good stability was observed during a preliminary 50 h measurement. These results demonstrate that $L_{0.3}$SFNM could be a promising alternative as symmetrical electrodes in SOECs for pure CO_2 electrolysis.

References:

[1] ALBO J, ALVAREZ-GUERRA M, CASTAÑO P, *et al*. Towards the electrochemical conversion of carbon dioxide into methanol. *Green Chemistry*, 2015, **17(4):** 2304–2324.

[2] FREUND H J, ROBERTS M W. Surface chemistry of carbon dioxide. *Surface Science Reports*, 1996, **25(8):** 225–273.

[3] ZHENG Y, WANG J, YU B, *et al*. A review of high temperature co-electrolysis of H_2O and CO_2 to produce sustainable fuels using solid oxide electrolysis cells (SOECs): advanced materials and technology. *Chem. Soc. Rev.*, 2017, **46(5):** 1427–1463.

[4] LIU S, LIU Q, LUO J L. CO_2-to-CO conversion on layered perovskite with *in situ* exsolved Co-Fe alloy nanoparticles: an active and stable cathode for solid oxide electrolysis cells. *Journal of Materials Chemistry A*, 2016, **4(44):** 17521–17528.

[5] SINGH V, MUROYAMA H, MATSUI T, *et al*. Feasibility of alternative electrode materials for high temperature CO_2 reduction on solid oxide electrolysis cell. *Journal of Power Sources*, 2015, **293:** 642–648.

[6] YUE X L, IRVINE J T S. Alternative cathode material for CO_2 reduction by high temperature solid oxide electrolysis cells. *Journal of the Electrochemical Society*, 2012, **159(8):** F442–F448.

[7] LI Y, CHEN X, YANG Y, *et al*. Mixed-conductor $Sr_2Fe_{1.5}Mo_{0.5}O_{6-\delta}$ as robust fuel electrode for pure CO_2 reduction in solid oxide electrolysis cell. *ACS Sustainable Chemistry & Engineering*, 2017, **5(12):** 11403–11412.

[8] LÜ H, LIN L, ZHANG X, *et al*. *In situ* investigation of reversible exsolution/dissolution of CoFe alloy nanoparticles in a Co-doped $Sr_2Fe_{1.5}Mo_{0.5}O_{6-\delta}$ cathode for CO_2 electrolysis. *Advanced Materials*, 2020, **32(6):** 1906193.

[9] YUE X, IRVINE J T S. Modification of LSCM-GDC cathodes to enhance performance for high temperature CO_2 electrolysis using solid oxide electrolysis cells (SOECs). *Journal of Materials Chemistry A*, 2017, **5(15):** 7081–7090.

[10] LU L, NI C, CASSIDY M, *et al*. Demonstration of high performance in a perovskite oxide supported solid oxide fuel cell based on La and Ca co-doped $SrTiO_{3-\delta}$ *Journal of Materials Chemistry A*, 2016, **4(30):** 11708–11718.

[11] QI W, GAN Y, YIN D, *et al*. Remarkable chemical adsorption of manganese-doped titanate for direct carbon dioxide electrolysis. *Journal of Materials Chemistry A*, 2014, **2(19):** 6904–6915.

[12] LIU S, LIU Q, LUO J L. Highly stable and efficient catalyst with *in situ* exsolved Fe-Ni alloy nanospheres socketed on an oxygen deficient perovskite for direct CO_2 electrolysis. *ACS Catalysis*, 2016, **6(9):** 6219–6228.

[13] TIAN Y, ZHANG L, LIU Y, *et al*. A self-recovering robust electrode for highly efficient CO_2 electrolysis in symmetrical solid oxide electrolysis cells. *Journal of Materials Chemistry A*, 2019, **7(11):** 6395–6400.

[14] LI Y, ZHAN Z, XIA C. Highly efficient electrolysis of pure CO_2 with symmetrical nanostructured perovskite electrodes. *Catalysis Science & Technology*, 2018, **8(4):** 980–984.

[15] ZHANG Y Q, LI J H, SUN Y F, *et al*. Highly active and redox-stable Ce-doped LaSrCrFeO based cathode catalyst for CO_2 SOECs. *ACS Applied Materials Interfaces*, 2016, **8(10):** 6457–6463.

[16] SÃNCHEZ D, ALONSO J A, GARCÍA-HERNÁNDEZ M, *et al*. Microscopic nature of the electron doping effects in the double perovskite $Sr_{2-x}La_xFeMoO_6$($0 \leqslant x \leqslant 1$) series. *Journal of Materials Chemistry A*, 2003, **13(7):** 1771–1777.

[17] SUGAHARA T, OHTAKI M, SOUMA T. Thermoelectric properties of double-perovskite oxide $Sr_{2-x}M_xFeMoO_6$ (M=Ba, La). *Journal of Ceramic Society Japan*, 2008, **116(1360):** 1278–1282.

[18] YANG X, CHEN J, PANTHI D, *et al*. Electron doping of $Sr_2FeMoO_{6-\delta}$ as high performance anode materials for solid oxide fuel cells. *Journal of Materials Chemistry A*, 2019, **7(2):** 733–743.

[19] AZIZI F, KAHOUL A, AZIZI A. Effect of La doping on the electrochemical activity of double perovskite oxide Sr_2FeMoO_6 in alkaline medium. *Journal of Alloys and Compounds*, 2009, **484(1/2):** 555–560.

[20] YANG X, PANTHI D, HEDAYAT N, *et al*. Molybdenum dioxide as an alternative catalyst for direct utilization of methane in tubular solid oxide fuel cells. *Electrochemistry Communications*, 2018, **86:** 126–129.

[21] SARMA D D, MAHADEVAN P, DASGUPTA T S, *et al*. Electronic structure of $Sr_2FeMoO_{6-\delta}$. *Physical Review Letter*, 2000, **85(12):** 2549–2552.

[22] LIU Q, DONG X, XIAO G, *et al*. A novel electrode material for symmetrical SOFCs. *Advanced Materials*, 2010, **22(48):** 5478–5482.

[23] DAI N, FENG J, WANG Z, *et al*. Synthesis and characterization of B-site Ni-doped perovskites $Sr_2Fe_{1.5-x}Ni_xMo0.5O_{6-\delta}$ (x = 0, 0.05, 0.1, 0.2, 0.4) as cathodes for SOFCs. *Journal of Materials Chemistry A*, 2013, **1(45):** 14147–14153.

[24] LU X, YANG Y, DING Y, *et al*. Mo-doped $Pr_{0.6}Sr_{0.4}Fe_{0.8}Ni_{0.2}O_{3-\delta}$ as potential electrodes for intermediate-temperature symmetrical solid oxide fuel cells. *Electrochimica Acta*, 2017, **227:** 33–40.

[25] PENG X, TIAN Y, LIU Y, *et al*. An efficient symmetrical solid oxide electrolysis cell with LSFM-based electrodes for direct electrolysis of pure CO_2. *Journal of CO_2 Utilization*, 2020, **36:** 18–24.

[26] WANG R, DOGDIBEGOVIC E, LAU G Y, *et al*. Metal-supported solid oxide electrolysis cell (MS-SOEC) with significantly enhanced catalysis. *Energy Technology*, 2019, **7(5):** 1801154–1801166.

[27] CAO Z, WEI B, MIAO J, *et al*. Efficient electrolysis of CO_2 in symmetrical solid oxide electrolysis cell with highly active $La_{0.3}Sr_{0.7}Fe_{0.7}Ti_{0.3}O_3$ electrode material. *Electrochemistry Communications*, 2016, **69:** 80–83.

[28] TIAN Y, ZHENG H, ZHANG L, *et al*. Direct electrolysis of CO_2 in symmetrical solid oxide electrolysis cell based on $La_{0.6}Sr_{0.4}Fe_{0.8}Ni_{0.2}O_{3-\delta}$ electrode. *Journal of The Electrochemical Society*, 2018, **165(2):** F17–F23.

[29] YANG Z, MA C, WANG N, *et al*. Electrochemical reduction of CO_2 in a symmetrical solid oxide electrolysis cell with $La_{0.4}Sr_{0.6}Co_{0.2}Fe_{0.7}Nb_{0.1}O_{3-\delta}$ electrode. *Journal of CO_2 Utilization*, 2019, **33:** 445–451.

[30] XU S, LI S, YAO W, *et al*. Direct electrolysis of CO_2 using an oxygen-ion conducting solid oxide electrolyzer based on $La_{0.75}Sr_{0.25}Cr_{0.5}Mn_{0.5}O_{3-\delta}$ electrode. *Journal of Power Sources*, 2013, **230:** 115–121.

[31] ADDO P K, MOLERO-SANCHEZ B, CHEN M, *et al*. CO/CO_2 study of high performance $La_{0.3}Sr_{0.7}Fe_{0.7}Cr_{0.3}O_{3-\delta}$ reversible SOFC electrodes. *Fuel Cells*, 2015, **15(5):** 689–696.

[32] LU C, NIU B, YI W, *et al*. Efficient symmetrical electrodes of $PrBaFe_{2-x}Co_xO_{5+\delta}$ (x=0, 0.2, 0.4) for solid oxide fuel cells and solid oxide electrolysis cells. *Electrochimica Acta*, 2020, **358:** 136916–136927.

$La_xSr_{2-x}Fe_{1.5}Ni_{0.1}Mo_{0.4}O_{6-\delta}$ 对称电池电解 CO_2 研究

王 玥[1,2], 崔常松[1,2], 王士维[1,2], 占忠亮[1,2,3]

(1. 中国科学院 上海硅酸盐研究所, 上海 200050; 2. 中国科学院大学, 北京 100049; 3. 中国科学技术大学 化学与材料科学学院, 合肥 230026)

摘 要:固态氧化物电解池(SOECs)因较高的能量转化效率在电化学还原 CO_2, 实现“碳中和”社会方面备受关注。与非对称电池结构相比, 对称 SOECs 的空气极和燃料极是相同或相近的材料, 可以减少界面种类, 改善电极与电解质的热膨胀匹配性, 简化电池的制备工艺。本研究合成了钙钛矿氧化物 $La_xSr_{2-x}Fe_{1.5}Ni_{0.1}Mo_{0.4}O_{6-\delta}$ (L_xSFNM, x=0.1、0.2、0.3、0.4), 作为固体氧化物电解池的对称电极用于评估纯 CO_2 的电化学还原性能。掺入 La^{3+}可以有效提高反应催化活性, 其中 $L_{0.3}$SFNM 为电极的电解池表现出最高的电化学性能, 800 ℃下, 在空气中的极化电阻为 0.07 Ω·cm^2, 在 50% CO-50% CO_2 中的极化电阻为 0.62 Ω·cm^2。单电池 $L_{0.3}$SFNM@LSGM|LSGM|$L_{0.3}$SFNM@LSGM 在 800 ℃和 1.5 V 电压下的电解电流密度为 1.17 A·cm^{-2}, 在初始的 50 h CO_2 短期电解测试中表现出优异的稳定性, 是一种理想的对称电极材料。

关 键 词: 对称固体氧化物电解池; 钙钛矿结构; 电极材料

中图分类号: TQ174　　**文献标志码**: A